The formation of Fe colloids and layered double hydroxides as sequestration agents in the natural remediation of mine drainage

Chikanda, Frances
Division of Sustainable Resource Engineering, Graduate School of Engineering, Hokkaido University

Otake, Tsubasa
Division of Sustainable Resource Engineering, Faculty of Engineering, Hokkaido University

Koide, Aoi
Division of Sustainable Resource Engineering, Graduate School of Engineering, Hokkaido University

Ito, Akane
Department of Applied Chemistry for Environment, School of Science and Technology, Kwansei Gakuin University

他

https://hdl.handle.net/2324/7173533

The formation of Fe colloids and layered double hydroxides as sequestration agents in the natural remediation of mine drainage

Frances Chikanda [a,*], Tsubasa Otake [b], Aoi Koide [a], Akane Ito [c], Tsutomu Sato [b]

[a] Division of Sustainable Resource Engineering, Graduate School of Engineering, Hokkaido University, N13W8, Kita-ku, Sapporo 0608628, Japan
[b] Division of Sustainable Resource Engineering, Faculty of Engineering, Hokkaido University, N13W8, Kita-ku, Sapporo 0608628, Japan
[c] Department of Applied Chemistry for Environment, School of Science and Technology, Kwansei Gakuin University, Gakuen2-1, Sanda, Hyogo 6691337, Japan

HIGHLIGHTS

- Fe colloids are formed from ferrous Fe in a circumneutral mine drainage.
- Core-shell ferrihydrite aggregates incorporate As thereby aiding in As removal.
- Seasonal colloid transportation is evaluated based on the aggregation rates.
- Zn-Fe layered double hydroxides are sequestration media for Zn from the drainage.
- Natural remediation is attained by Fe colloids and layered double hydroxides.

GRAPHICAL ABSTRACT
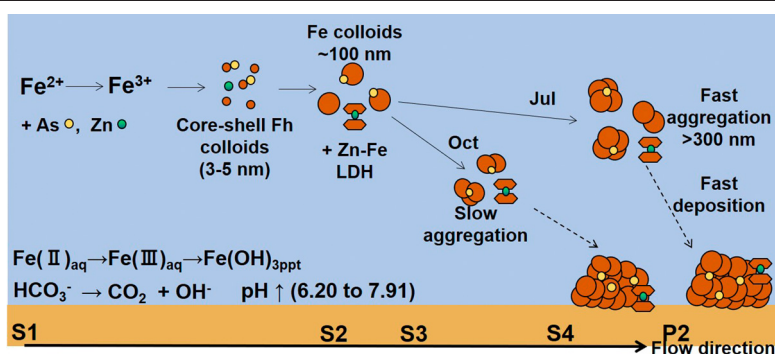
ABSTRACT

The increasing need to treat wastewater from mine effluents has drawn attention to passive treatment systems. Colloids are common in mine waters and are highly reactive, so their formation, characteristics, behavior, and the critical factors that affect them need to be understood for designing efficient treatment systems. An investigation was conducted at the abandoned Ainai mine drainage, Japan, where aeration is utilized to remove Fe, As, and Zn from circumneutral wastewater drainage, during rainy and dry seasons of 2016 and 2018 respectively, based on observations of physiochemical characteristics, elemental concentrations in dissolved and colloidal fractions, transmission electron microscopy, and synthetic experiments. In this circumneutral Fe-rich mine drainage, Fe^{2+} is oxidized to Fe^{3+}, resulting in the formation of Fe colloids that incorporate As during their formation. Colloid formation increases turbidity, and, in the rainy season, increased colloidal interaction enhances their aggregation and higher flow rates lead to greater mobilization of the colloids. Zn-bearing colloids are rare in Ainai mine drainage because the Zn concentrations are low. However, Zn-Fe layered double hydroxide (LDH) was identified and confirmed by geochemical modelling and experiments. The Zn-Fe LDH was formed by isomorphous substitution of Zn into an $Fe^{2+}-Fe^{3+}-CO_3^{2-}$ LDH, at pH greater than 7.5, thereby achieving efficient natural remediation of Zn and As in the drainage.

1. Introduction

Mine drainage is an increasing source of toxic elements in the environment (Fu and Wang, 2011), due to wastewater released from underground workings or tailings. Various treatment methods have been applied to treat such wastewater, all involving long-term and

* Corresponding author.
 E-mail address: franceschikanda2@gmail.com (F. Chikanda).

expensive processes, so natural remediation processes, (i.e., passive treatment systems), are becoming the preferred option (Zipper and Skousen, 2014). Geochemical characteristics of wastewater such as pH, redox conditions, dissolved chemical composition, and organic-matter content (Nordstrom, 2011) vary at different sites, as well as in different seasons. As a consequence, it is necessary for designing efficient treatment systems, to understand the processes and factors that affect natural remediation. The most common types of mine drainage wastewaters are acidic (Dold, 2014), and these have been studied in more detail than their circumneutral counterparts. To achieve remediation, most acidic mine drainage is mixed with other water sources to attain a circumneutral pH (Jung et al., 2012), but field studies highlighting processes that may achieve effi-cient remediation are scarce, especially those concerning nanoparti-cle behavior and seasonal variations.

Iron is generally ubiquitous in mine drainage, along with other toxic elements (Pokrovsky and Schott, 2002; Schemel et al., 2000). The ther-modynamic characteristics of Fe allows it to affect the mobility of toxic elements such as arsenic (As), zinc (Zn), lead (Pb), and copper (Cu), be-cause it exists as Fe^{2+} in relatively anoxic environments but can oxidize to Fe^{3+} and form Fe oxyhydroxides under oxidizing conditions (Whitney King, 1998). In oxic and neutral-pH environments, Fe^{3+} exists predominantly in the oxyhydroxide form, facilitating the formation of Fe-rich colloids (1 nm to 100 nm) (Liao et al., 2017; Gledhiir and Buck, 2012). Considering the abundance and large surface area of colloids, Jung et al. (2012) reported that Fe colloids are more reactive than bulk suspended solids, and their sequestration of other toxic elements has been widely reported. Experimental studies have also highlighted this (Sharma et al., 2010; Mokhter et al., 2018). However, due to the diverse geochemical characteristics of treatment systems, field evidence concerning the formation and behavior of Fe colloids, and their signifi-cance in removing toxic elements from mine drainage, still requires clarity.

Colloids are resistant to gravitational settling, and studies of their formation and aggregation rates should account for the time they re-main in the system (Pokrovsky and Schott, 2002; Wang et al., 2014). Whereas deposition of colloids is possible once the aggregates become large enough, aggregation rates may vary between systems and de-pending on the aqueous chemistry. The estimation of aggregation rate is therefore a major aspect to consider in the design of passive treatment systems.

Processes such as competitive adsorption and precipitation kinetics in mine drainage usually result in the formation of a variety of mineral phases that are able to sequester toxic elements (Plumlee et al., 1997; Nguyen et al., 2019). In addition to Fe colloids as a dominant medium for remediation, layered double hydroxides (LDHs) have also gained popularity due to their efficiency, flexibility, and ability to reduce con-centrations of metals such as Zn and Cu (Xu, 2013; Okamoto et al., 2010). Previous studies have reported natural occurrences of LDHs and their synthesis, particularly in the presence of Fe (Morimoto et al., 2015; Hongo et al., 2008). However, clarity is still lacking regarding the characterization of LDHs and factors crucial for their formation and stability, as might be provided by comparisons of field and experi-mental observations.

Here we report a study of a circumneutral passive treatment sys-tem utilizing aeration to remove Fe, As, and Zn from underground wastewater drainage from Ainai mine, Japan, considering both dis-solved and colloidal fractions. The progression of elements from dis-solved to colloidal states and their ultimate fate were studied. Our objectives were to (1) clarify the formation, semi-quantitative ag-gregation, and deposition behaviors of Fe colloids at circumneutral pH; (2) examine their application to As and Zn sequestration from mine drainage over two seasons; and (3) investigate the formation of LDHs by comparing natural and synthetic samples and factors af-fecting their formation and stability. The concentrations of metals in the drainage system from the mine provided insight into the

behavior of the metals involved, and highlighted factors that deter-mine the fate of toxic elements in mine drainage.

2. Materials and methods

2.1. Study area

The abandoned Ainai mine is in the northern part of Kosaka town, ~600 m northeast of Omori mountain, in the Hokuroku district, Akita prefecture, Japan. Sulfide ores containing Zn, Pb, and Cu (e.g., sphalerite, galena, chalcopyrite) were mined from the Kuroko-type volcanogenic massive sulfide deposit (1951 to 1985), which was formed associated with submarine bimodal volcanisms in the middle Miocene (Ishii, 1964; Yamada and Yoshida, 2011). Contaminated water has flowed from the mine since its closure and requires treatment before discharge. Aeration has been used to oxidize and precipitate Fe along with As and Zn. This natural remediation involves a 1000 m drain that runs from the underground tunnel through two treatment ponds to con-nect with a tributary of the Kosaka River at altitudes of 260–300 m (Fig. 1a). Wastewater flows from the underground mine in pipes (Fig. 1b), through a concrete drain inside a tunnel (Fig. 1c), is released to an outside drain (Fig. 1d), which has steps to improve aeration (Fig. 1e), then connects to a concrete drain (Fig. 1f) before being stored in a reservoir (Fig. 1g) and sedimentation ponds prior to release to the river. Sediments that accumulate in the ponds are transferred periodically to a nearby area.

Ainai mine drainage is located in a sub-frigid humid climate, with four distinct seasons. Abundant snowfall and monsoons have been reported in the region (Lu et al., 2019). Besides winter, when the drainage is covered by snow, precipitation at Ainai is highest in July, and lowest in October (Fig. S1a). Snow falls from October until mid-February (Japan Meteoro-logical Agency, 2018). Therefore, July and October are referred to as the rainy and dry seasons, respectively, at some points in the manuscript for simplicity.

2.2. Sampling and on-site measurements

Field surveys at Ainai mine were conducted annually from 2016 to 2019, however, the data reported here are from the surveys that were conducted in July 2016 and Oct 2018. These datasets are a representa-tive summary of our findings. Sixteen samples of water, suspended solids, and sediments were collected from the tunnel exit at the upper drain (S1; Fig. 1a), at ~100 m intervals until S6, and from the reservoir and settling pond (P1 and P2, respectively, Fig. 1a).

Water was sampled through three types of filters, 0.2 μm PTFE mem-brane filter (Advantec 25HP020AN), 200 kDa ultrafilter (Advantec USY-20) and As filters (Sep-Pack cartridge: As exchange column), to provide four types of sample: 0.2 μm membrane-filtered, non-acidified sample for anion determinations; acidified 0.2 μm membrane-filtered sample; and 200 kDa ultra-filtered sample and samples to be analyzed for As speciation, with the latter three being acidified by 1 vol% HNO_3 (ultra-pure grade, Kanto chemicals) for cation determinations. Here, we define the dissolved and colloidal fractions as follows: (1) ultrafiltered water samples contain the dissolved fraction; (2) membrane-filtered samples contain the colloidal and dissolved fractions; (3) the difference between (1) and (2) provides the colloidal fraction. Samples were collected in 50 mL polypropylene bottles, pre-rinsed with 3 vol% HNO_3 overnight, and stored at ~4 °C pending analysis. Sediments were also collected at all sampling points S1 to S6. Suspended particulates were also collected at all points until P1 (Fig. 1a) by pumping 0.5 L of water through 0.2 μm mixed-cellulose-ester filters (Advantec A020A047A). On-site measure-ments were undertaken for Fe^{2+} concentrations, dissolved oxygen (DO), pH, electrical conductivity (EC), turbidity, temperature, oxidation-reduction potential (ORP), and alkalinity of water samples. A pack test was used for Fe^{2+} concentrations; Eh (Redox potential of the normal hydrogen electrode) was calculated as Eh = E+206-
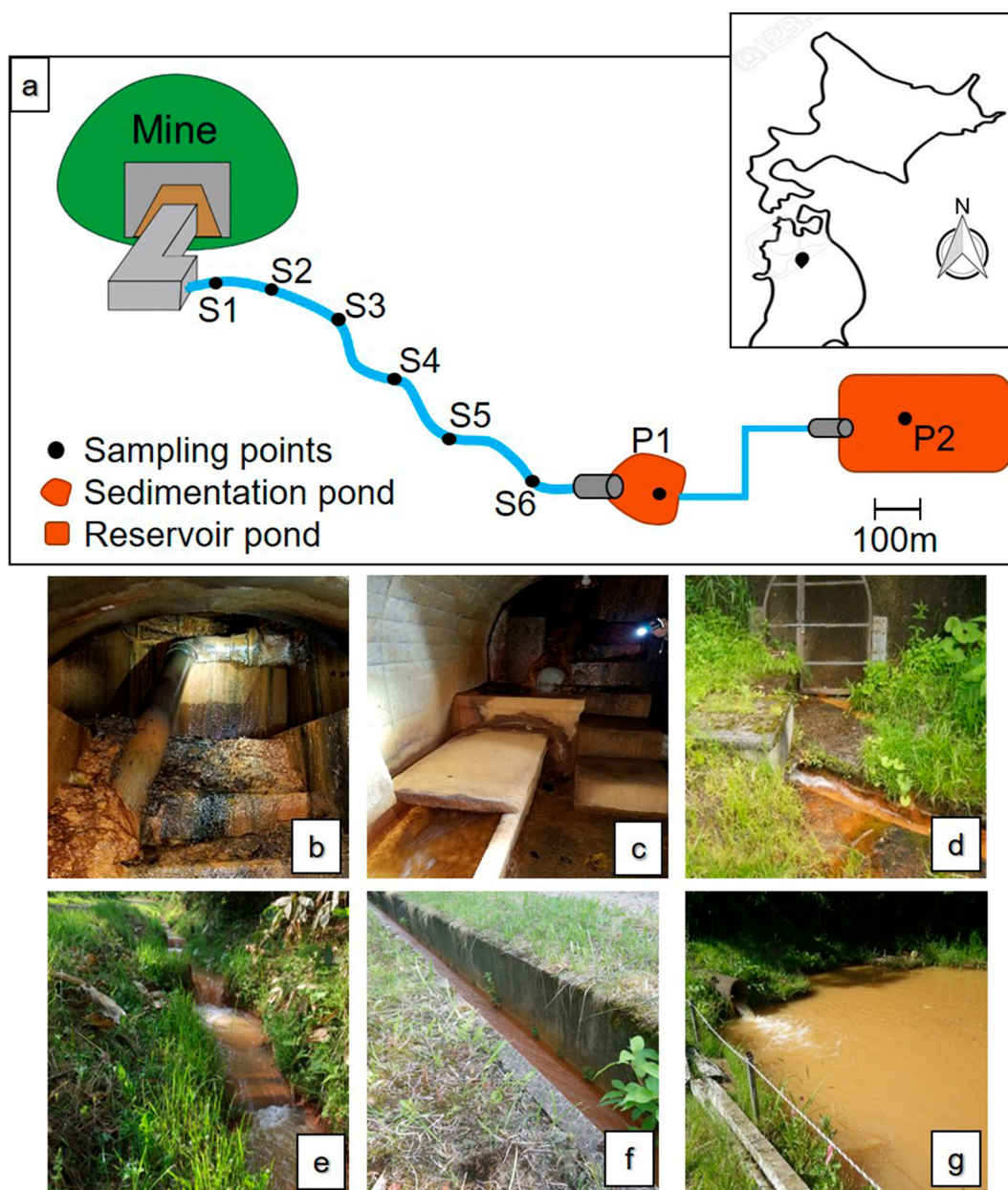
Fig. 1. (a) A schematic representation of Ainai mine drainage showing the sampling points (S1–S6), reservoir (P1), and settling pond (P2) with an inset map showing the location in Japan; (b) pipe releasing water from underground to concrete drain; (c) concrete drain inside the tunnel; (d) upper exterior drain (S1); (e) unconcreted upper to middle drain, (f) concreted lower drain; (g) reservoir pond (P1).

$0.7 \times$ (T-25) (E: oxidation - reduction potential (mV), T: temperature (°C)). Alkalinity was determined by HNO_3 titration of water samples filtered through a 0.45 μm PTFE membrane filter. A Gran-function plot was applied to obtain HCO_3^- concentrations from the alkalinity (Rounds and Wilde, 2006). Distances from each sampling site and flowrates were measured on site.

2.3. Analytical methods

Non-acidified water samples were diluted 10 times and analyzed by ion chromatography (IC; Metrohm IC861) using Multi-anion Standard Solution 1 (Wako Pure Chemical Corporation) for calibration. Acidified samples were diluted 40 times and analyzed for major and trace elements by inductively coupled plasma–atomic emission spectroscopy (ICP–AES; Shimadzu ICPE-9000) and ICP–mass spectrometry (ICP–MS;

Thermo Scientific iCap Qc). Standards were prepared from a multi-standard solution (Wako). In, Ru and Rh and were used as internal standards for ICP–MS analysis. Oxide formation during analysis was monitored by the CeO/Ce ratio and maintained at <0.5% and He collision mode was utilized to avoid molecular interference from $^{40}Ar^{35}Cl^+$ on $^{75}As^+$.

Sediment and suspended particulate samples were dried at room temperature and the minerals present were determined by X-ray diffraction (XRD; Rigaku XRD Multi-Flex) using Cu Kα radiation (λ = 0.15406 nm) with an accelerating voltage of 30 kV and beam current of 20 mA, in the 5°–70° range, scanned at 2.0° min^{-1}. The morphology and chemical composition of the suspended particulates were analyzed by field-emission scanning electron microscopy with an energy-dispersive X-ray spectrometer (FE–SEM–EDS; JEOL JSM-6500F). Samples were prepared for transmission electron microscopy (TEM; JEOL

JEM-2010) by dispersion in ethanol (with ultrasonication) and placed on a Cu grid with a film. Minerals were identified using Crystal Structures Libraries.

2.4. Synthesis of Zn-bearing colloids and thermodynamic calculations

The mineralogical characteristics of solid samples were studied to constrain sequestration mechanisms for toxic elements. Zinc concentrations in the aqueous solutions from the drain may have been too low to produce observable amounts of Zn-bearing colloids in the sediments by the above methods. Therefore, $ZnSO_4 \cdot 7H_2O$ was added to wastewater collected in 2 L bottles to induce the synthesis of Zn-bearing minerals. With reference to previous studies (Morimoto et al., 2015; Parida and Mohapatra, 2012) and based on Ainai mine water chemistry, synthesis was done using unfiltered water sample from S1 (Fig. 1a) to act as a supply of Fe, and addition of $ZnSO_4 \cdot 7H_2O$ to increase the Zn concentration. The Zn reagent (249.5 mg) was added to 2 L of sample to provide a Zn:Fe molar ratio of 2:1. The samples were stirred and allowed to settle for 24 h at room temperature, after which precipitates were collected on 0.2 μm filters for XRD and SEM analysis. The Zn and Fe concentrations (by ICP–AES) and pH were recorded immediately after mixing and again after the 24 h.

Stability diagrams for possible mineral forms expected in the drainage were constructed using the Geochemist's Workbench software (GWB model, Ver. 14) to evaluate their formation in the drainage at various pH values. Measured element concentrations were used as input parameters for modelling to account for the effects of coexisting cations and anions on solubility. Solubility diagrams were constructed using thermodynamic datasets generated from the thermoddem, modified where necessary by additions from the literature, in particular incorporating layered double hydroxides and other iron oxides (Bravo-Suárez et al., 2004). Interlamellar anions, combinations of divalent and trivalent cations, and related species, cause wide variations in the chemical compositions of LDHs. Therefore, the solubility products of Zn-Fe LDHs were estimated using the chemical compositions and thermodynamic data of the end-member hydroxides, sulfates, and carbonates (Allada et al., 2006). Thermodynamic data for these compounds were referred from the enthalpies of formation measured by acid-solution calorimetry, and solubility products were based on solubility measurements (Bravo-Suárez et al., 2004; Hase et al., 2017).

3. Results and discussion

3.1. General characteristics of water samples

Results of on-site measurements of Ainai mine drainage are reported in Supplementary Table S1. Based on the stiff diagram (Fig. 2a), the water samples are classified as Ca–SO₄-type water, indicating mixing of mine drainage with underground water rich in Ca and HCO_3^- before outflow from the mine head (Akashima et al., 2011). Despite being

unusual for mine drainage, this classification was observed from the upper to the lower drain with negligible variations, implying that external factors have no significant effect on the drainage system. The HCO_3^- concentration is relatively high and decreased down-drain (246.2 to 127.1 mg L^{-1}), indicating a strong buffering capacity. Ainai mine drainage is a neutral to alkaline (pH 6.20 to 7.91) system and pH increases down-drain with decreasing HCO_3^- (Fig. 2b). This inverse relationship reflects CO_2 degassing by aeration (Kirby et al., 2007), and the dissociation of HCO_3^- to CO_2 and OH^- ion (Langmuir, 1997). Unlike most mine drainages, which are actually acidic, Ainai mine drainage is circumneutral despite an abundance of SO_4^{2-} in the system and this is due to the mixing of the drainage in the underground. Ainai mine drainage is generally an oxidative system, with over saturation of DO (6.54–12.55 mg L^{-1}), possibly attributable to microbial photosynthesis (Stumm and Morgan, 2006). ORP values increase from the upper to lower drain (127 to 209 mV), possibly due to increasing pH (Stumm and Morgan, 2006). These properties exhibit negligible variation between July and October. However, the flow rate, turbidity, and Fe^{2+} concentrations display notable variations between the two months (Supplementary Table S1), with average flow rates of 32.80 and 22.96 L s^{-1} in July and October, respectively, which is attributed to heavier precipitation in July (Fig. S1a).

3.2. Relationship between Fe colloids and turbidity

The turbidity is generally higher in July, when rainfall and flow rates are high, than in October (Fig. 3a), while Fe^{2+} concentrations are lower in July than October (Fig. 3b) as a result of dilution by higher precipitation rates. There is an inverse relationship between turbidity and Fe^{2+} concentrations (Fig. S1b); turbidity increases and Fe^{2+} concentrations decrease down-drain. Turbidity is commonly higher in rainy seasons mainly due to the resuspension of sediments (Zay Ya et al., 2020; Rezaei et al., 2013). The higher precipitation at Ainai may have further contributed to geochemical processes in the drainage, with the inverse relationship between turbidity and Fe^{2+} concentration indicating oxidation of Fe^{2+} to Fe^{3+} ion (Nairn et al., 2002), thereby facilitating formation of nanoparticles (Buffle and Leppard, 1995) with increasing turbidity (Tikhonova, 2016; Yao et al., 2014). This process typically occurs in circumneutral pH systems, as in this case.

In the Ainai drainage, the abundance of Fe and trend of decreasing Fe^{2+} imply the formation of nanoparticles of Fe colloid (oxy)hydroxides, whose mobility and perhaps aggregation behavior might be reflected by the turbidity. The turbidity continues to increase further down-drain in July, in contrast to the decrease observed in October when the flow rate is lower, indicating more rapid formation and/or aggregation of precipitates in the rainy season (July). The increasing turbidity supports the notion that the precipitates were mobilized over greater distances during the rainy season, indicating that flow rate should be a significant factor for consideration in the design of passive treatment systems. Turbidity increases with particle size (Tikhonova,
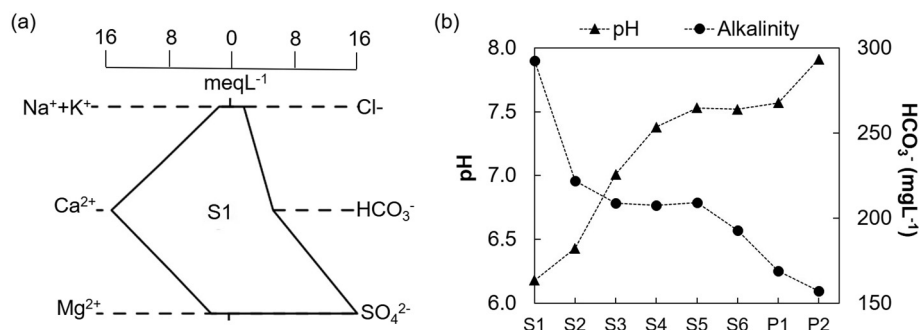
Fig. 2. Average fluid compositions for July and October; (a) stiff diagram and (b) down-drain pH and HCO_3^- trends.
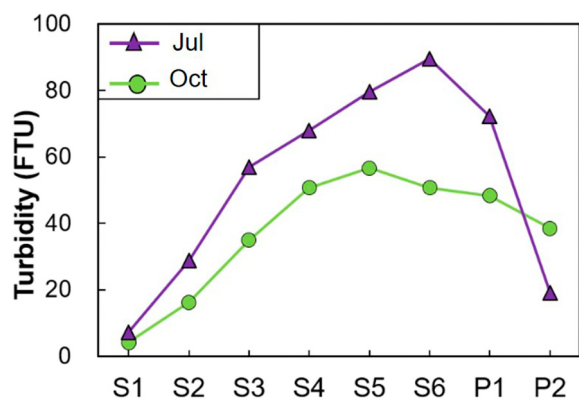
Fig. 3. Trend displayed by turbidity in July and October.

2016; Yao et al., 2014), implying more aggregation of Fe colloids in the rainy season, such that increased interaction among the colloids overcomes repulsive forces between them (Petosa et al., 2010; Baalousha, 2009), leading to more aggregation. At P1 and P2 (Fig. 1a), turbidity decreases markedly, because of the longer residence time and sedimentation in the ponds (Fig. S2); the larger particles in July settled more quickly with a greater drop in turbidity than in October. The calculated charge imbalance for all water samples was within ±15%.

3.3. Distribution of Fe, As, and Zn in dissolved and colloidal fractions of mine drainage

Fe, As, and Zn concentrations in dissolved and colloidal fractions of water samples are reported in Supplementary Table S2 and plotted in Fig. 4. The dissolved Fe concentration decreases down-drain (12.1 mg L^{-1} at S1 to 0.015 mg L^{-1} at P2), most notably between S1 and S3 where it is almost completely replaced by colloidal Fe, which forms increasingly as flow proceeds downward (Fig. 4a). The concentration of dissolved Fe fraction is similar to the Fe^{2+} concentration (Fig. S1) obtained by on-site pack tests, therefore implying that the dissolved Fe fraction is predominantly Fe^{2+}. Subsequently, colloidal Fe forms in the

upper drain, initiated by the oxidation of Fe^{2+} to Fe^{3+} and allowing the formation of the Fe hydroxide nanoparticles (Pokrovsky and Schott, 2002). The nanoparticles are prone to aggregating (Kellner and Köhler, 2005) with increasing particle size, and the turbidity increase (Fig. 3) is attributed to the formation of Fe colloids (Liao et al., 2017). Despite the increase in the colloidal Fe fraction (1.39 mg L^{-1} at S1 to 8.79 mg L^{-1} at S2), at the expense of dissolved Fe, the total Fe concentration decreases down-drain (Fig. 4a) due to the aggregation of colloids to a size that is removed efficiently by gravitational settling, thereby removing the particles effectively from the drainage.

Arsenic, which is mainly Arsenite, As(III), throughout the drainage, shows a similar trend to Fe, most noticeably in the distribution between dissolved and colloidal fractions in the drain (Fig. 4b). Colloid formation is inferred at S2 and S3 (where Fe colloids also dominate) and total As continues to decrease down-drain, reflecting the impact of Fe colloids on As mobility. Conclusively, Fe colloids behave as the primary colloids, whereas As exists as pseudo-colloids, hence the fate of As being mainly determined by Fe colloids in the drainage (Fritzsche et al., 2011). The impact of Fe nanoparticles on As in aquatic systems has been studied previously (Zhao et al., 2011; Leupin and Hug, 2005), with several removal mechanisms being proposed, including co-precipitation of Fe hydroxides with As (Crawford et al., 1993; Yokoyama et al., 1999) and adsorption of As by Fe hydroxides (Khamphila et al., 2017). Considering the similar trends in Fe and As observed here, we suggest that As may be incorporated into the Fe colloids and removed from the mine drainage by co-precipitation and aggregation of the As containing Fe colloids. On the other hand, an inverse relationship where Fe concentrations in July are higher, while As concentrations are lower is observed. Higher Fe concentrations are most likely from the underground source, but the low As concentrations are associated with the increased Fe, which allows for more sorption of As, hence the inverse relationship also displayed in October when precipitation of As is lower due to higher Fe. However, further downstream, As remains in the drainage as the dissolved phase. Zeng (2003) reported a decreased affinity of iron oxides to As adsorption, that is associated with the less affinity of Si for the As, thereby leaving As in the drainage.

On the contrary, Zn and Si (Fig. 4c and d) display different trends from Fe and As in the drainage. They (Zn and Si) mainly exist as dissolved fractions and minimally removed from the drainage. There may
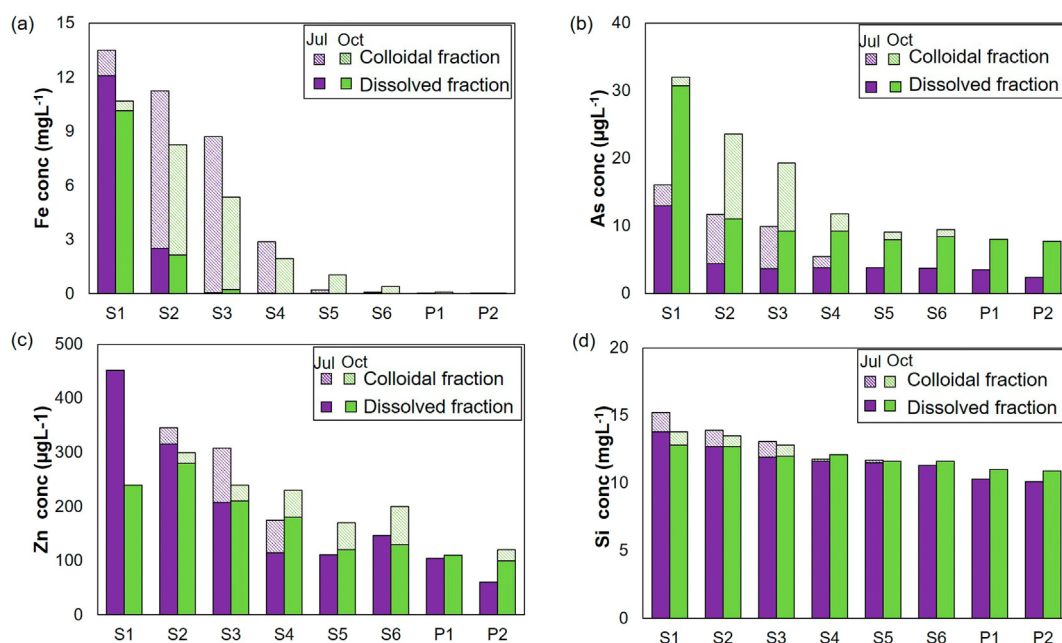

Fig. 4. Distribution of (a) Fe, (b) As, (c) Zn and (d) Si concentrations in the dissolved and colloidal fractions as a function of distance from the mine.

be various constraining factors that resist the colloid formation and removal of the elements in the drainage, and since the metal concentration patterns may be difficult to utilize as clarification tools, therefore, mineralogy and modelling was utilized to clarify the behaviors of these elements.

3.4. Mineral compositions and aggregation behavior of Fe colloids

Particles collected as colloids on the 200 kDa filters were further characterized by TEM and EDS. They display aggregated spherical structures (Fig. 5a), typical of Fe colloids (Liao et al., 2017; Gledhiir and Buck, 2012). The particles were more abundant on filters from sites S2 and S3, implying that formation of colloids occurred mainly in the upper drain, soon after oxidation of Fe^{2+} to Fe^{3+}. The composition of colloids was homogeneous throughout the drainage, including mainly Fe, Si, S, C, and O (Fig. 5b). As concentrations were too low to be detected by EDS. The colloids were likely Si-bearing 2-line ferrihydrite (Dold and Fontboté, 2002), as implied by XRD results of the suspended solids (shown in the following section), which has been reported to be stable, especially at pH ≥ 4, thus explaining the stability of Fe colloids formed in the Ainai mine drainage. This also reflects the minimal removal mechanism for Si from the drainage, showing that it is incorporated in the Ferrihydrite colloids.

The typical colloid aggregate particle-size range collected on the ultrafilter is 100–200 nm, and they have distinctive spherical shapes (Fig. 5a). This suggests that colloids remain suspended at around this size and are further transported in the drainage. However, since the dynamics of Fe oxides formations have reported that they are sometimes formed from smaller particles, the particles were further observed under TEM. Further enlargement by TEM (Fig. 5c) indicates that the colloids are aggregates of finer-grained particles of 3–5 nm diameter (Fig. 5d). The Fe colloidal particles under TEM exhibit two rings at 2.66 and 1.49 Å, consistent with those of core–shell ferrihydrite

(Weatherill, 2016). Core-shell ferrihydrite are precursors to ferrihydrite, which is a cluster of Fe ions that is a pre-nucleation cluster. These clusters have also reportedly been associated to the spherical structure borne by the ferrihydrite colloids (Michel, 2007). These observations show that the Fe colloids in the drainage, following oxidation, slowly generated into the spherical colloid aggregates observed on the ultrafilters.

Previous studies have indicated that nanoparticle aggregation is inevitable in liquid phases and significantly alters their properties, thereby affecting the stability of colloids (Petosa et al., 2010; Baalousha, 2009). The surface charge of colloids, which is impacted by pH of solution, anion concentrations and organic matter among other factors, enhances repulsive interactions, dispersing them in the liquid phase, but their continued interaction overcomes these forces, allowing their agglomeration. As the colloids also host As, their aggregation behavior, which gives insight into their mobility and deposition characteristics, was investigated semi-quantitatively.

Formation of the colloids in the drainage shows that, core–shell ferrihydrite (~3 nm) is evident in TEM micrographs (Fig. 5), implying that the collected colloids were actually aggregates formed from core-shell ferrihydrite, which then aggregate to spherical, stable 100 nm Fe hydroxide colloids. The increase in turbidity in Section 3.2 is thus a result of the aggregation of core–shell ferrihydrite to form 100 nm colloids. Given that these colloids were collected on the ultrafilters implies that they had not settled and remained in the drainage to a certain point. Since distances from one point to the next were measured during field sampling, a relation of the colloid concentrations with distance is reported in Fig. 6. Evidently from the graph, following their formation, the colloids formed at S1, S2 and S3 are transported down, while at S4, significant deposition is observed. This suggests that the colloids were aggregated to a particular size before deposition.

Observation of the colloids at different points of the drainage displayed variations in size and aggregation (Figs. S2 and S3). An
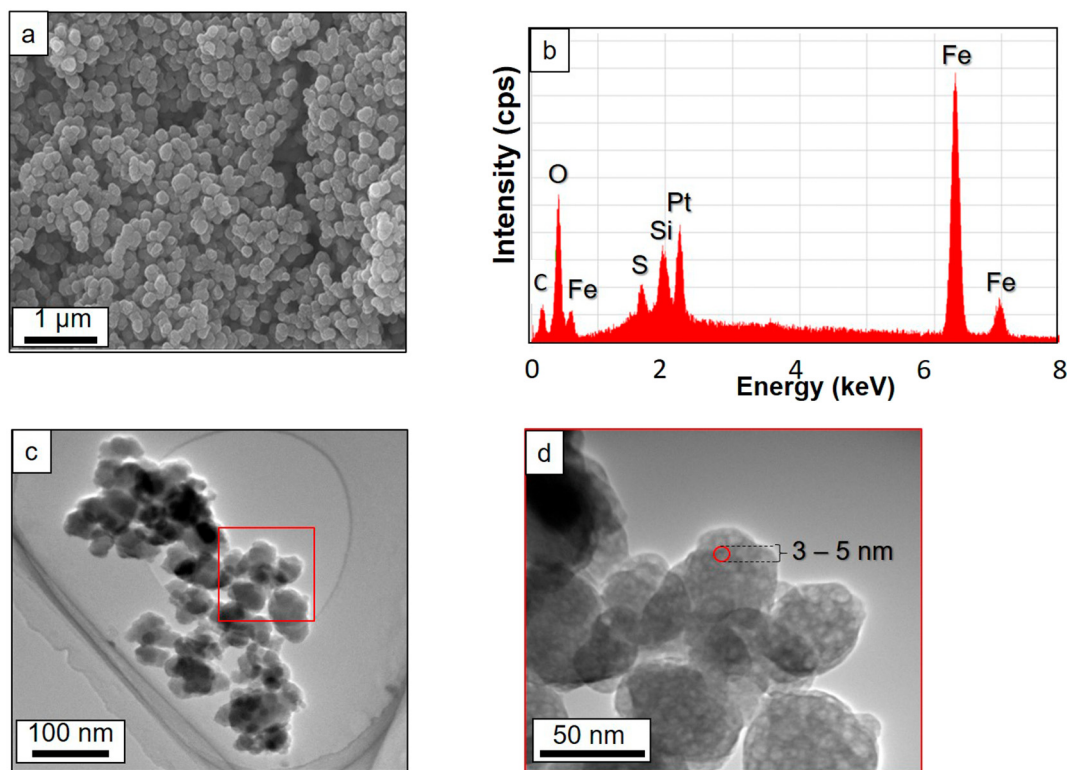
Fig. 5. Morphology and composition of colloids collected on 200 kDa ultrafilters. (a) Fe colloid aggregates formed in Ainai mine drainage; (b) EDS spectrum showing the composition of the colloids; (c) TEM image of aggregates of Fe colloids in the suspended solids at P1 and (d) an enlargement of the colloids under TEM (the sample was coated with Pt for SEM analysis).
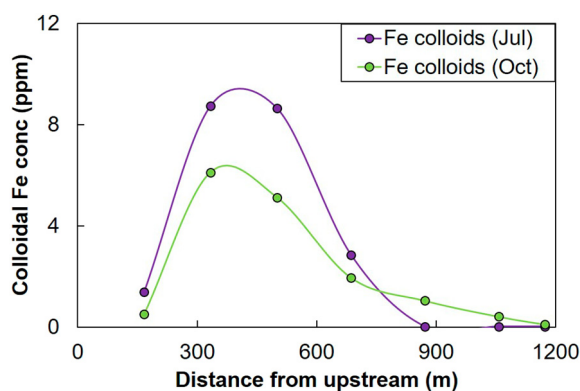
Fig. 6. Colloidal concentrations of Fe in July and October as a function of distance from the upstream.

increase in size from S1 to S4 in particular was measured following microscopic observations. A gradual increase in size and colloidal aggregates was observed; S1, S2 and S3 have a distribution of 80 to 300 nm colloid aggregates which increase in abundance from S1 to S3. On the other hand, S4 was majorly composed of highly aggregated colloids of 300–400 nm. Particle aggregates larger than 400 nm were not observed on the ultrafilters, implying that colloid aggregates of >400 nm were deposited to the bottom of the drainage. Subsequently, deposition of the colloids in the drainage occurs at ~300 to ~400 nm particle size indicating that the colloids are efficiently removed by gravitational settling when they reach a certain size.

The rate of aggregation in the drainage, as indicated by the turbidity, warrants study. The colloids in this system do not disintegrate after formation and are mobilized over considerable distances before deposition in the reservoir and sedimentation ponds. Colloid stability may be associated with Si in the system (Vempati et al., 1990), which allows formation of stable ferrihydrite. However, the aggregation rate may be explained by the DLVO theory, which highlights electrostatic factors affecting aggregation behavior. Given the high pH of the system, which results in the system being near the point of zero charge, aggregation of the particles is quite significant, hence the colloid deposition observed at about 500 m from their formation. According to the DLVO theory, repulsive forces limit aggregation, and this limitation is not so significant at Ainai mine drainage and aggregation is achieved to remove colloids from the drainage.

A variation in the aggregation rate in July and October exists. In July, the turbidity quickly increases, and also quickly decreases towards the downstream, whereas, in October, the turbidity slowly increases and remains at values lower than July for longer distances (Figs. 3 and 6). This indicates that in July, the colloids aggregate faster than in October and are deposited faster than in October. According to previous research, increased van der Waals forces (Hiemenz, 1972; Hunter, 1963) may be responsible for this phenomenon, seeing as in July, total Fe is more abundant in the drainage, allowing more colloid formation, therefore, interactions among colloids are also increased, and result in faster aggregation than October. Consequently, the larger aggregates reach an ideal settling size quickly in July, allowing for the quicker deposition of the As-bearing Fe colloids in July unlike in October.

3.5. Removal of Zn by colloid formation

Fe and As concentrations decrease steadily in response to colloid formation but Zn concentrations decrease in an irregular pattern. (Fig. 4c). Formation of Zn colloids is observed downstream from S2 as pH increases slightly, most likely because Zn colloid formation is highly pH-dependent (Roberts et al., 2002). A colloidal fraction is also observed at sites S3 and S4, but the total Zn concentration does not reduce significantly at these sites. Considering that the Fe concentration in the

drainage is significantly higher than that of As, and the high adsorption efficiency of ferrihydrite at circumneutral pH (Hao et al., 2018), the Fe in the drainage should be sufficient to remove the Zn. It follows that there must be other factors inhibiting Zn removal by colloids, possibly involving a different removal mechanism.

An FE–SEM observation coupled with EDS of natural suspended particles collected at P1 (Fig. 7a), besides minor calcite and gypsum, revealed layered particles containing Zn, Fe, Ca, Si, C, and O (Fig. 7b). Furthermore, XRD peaks of the same natural samples were observed at 2θ at around 12.2°, 20.1° and 59.5° corresponded to previously reported Zn-Fe LDHs (Zaher, 2020; Moaty et al., 2016) (Fig. 7c), further supported by a supplementary FTIR characterization (Fig. S4). These observations strongly suggest that an LDH is responsible for the removal of Zn from the mine drainage. Despite this finding, their occurrence was rare in the drainage and the particles were relatively small, implying a limited formation. Therefore, using the drainage water samples that the Zn reagent was added, the synthesized layered particles were obtained (Fig. 7d). Zn and Fe concentrations in the water sample decreased drastically after 24 h (Table S3) and showed significant particle formations. FE-SEM (Fig. 7d) and EDS of the synthesized particles also showed the presence of layered particles similar to those of the natural sample, with similar compositions. In addition, the abundance and size of the particles was much higher than those of the natural samples, implying that the Zn concentration may have limited the formation of Zn-Fe LDH in the drainage. Following the synthesis, in addition to more and larger Zn particles collected from the filtration of the sample, an increase in pH was observed (6.19 to 7.82). Our findings therefore suggest that Zn concentration and pH are critical factors in Zn sequestration from mine drainage.

Layered double hydroxides comprising trivalent and divalent cations and anions (Hase et al., 2017) remove toxic elements effectively from a variety of systems (Hase et al., 2017; Hao et al., 2018). Toxic metal ions can be removed from water by LDHs via: (i) precipitation of metal hydroxides onto their surface; (ii) adsorption through bonding with LDH surface hydroxyls; (iii) isomorphous substitution; and (iv) chelation with the functional ligands in the interlayers (Xu, 2013). The chemistry of Ainai mine drainage includes Fe^{3+} and Fe^{2+} cations and HCO_3^- and SO_4^{2-} anions. Coexisting Fe^{3+} and Fe^{2+} might have supported LDH formation, but HCO_3^-, the major anion in this drainage system, is an ideal candidate for LDH formation, unlike SO_4^{2-} because the abundance of HCO_3^- makes it more feasible than SO_4^{2-}. Therefore, we suggest the formation of an Fe^{2+}–Fe^{3+}–CO_3^{2-} LDH, in which Zn may be isomorphically substituted, as a remediation mechanism for the Ainai mine drainage, which quickly transforms to a stable phase composed of Zn, Fe, Ca, C and O i.e., Zn-Fe LDH.

The formation and stability of a Fe^{2+}–Fe^{3+}–CO_3^{2-} LDH were considered at various pH values by thermodynamic modelling using the GWB software (Fig. 8). The measured elemental concentrations in water samples at site S2 were used as input parameters for modelling to account for the effect of coexisting cations and anions on colloid solubility and separation. Bravo-Suarez (Bravo-Suárez et al., 2004) estimated solubility products of LDHs with different anions, based on their chemical compositions and thermodynamic data for their end-products. These data were used to model the formation of LDHs in the mine drainage. A gradual decrease in Fe^{2+} concentration occurs from the upper to lower drain, particularly at S3 Fig. 3b. In the Eh–pH stability diagram (Fig. 8), S3 and S4 plot near the equivalence state between ferrihydrite and the Fe^{2+}–Fe^{3+}–CO_3^{2-} LDH, implying that the LDH might have formed near S3 where pH and Eh are inferred to be controlled by coexisting ferrihydrite and Fe^{2+}–Fe^{3+}–CO_3^{2-} LDH. Although the possibility of Hydroxygreen rust (OH) formation is observed, the pH in this drainage does not reach 11, hence its formation is eliminated. The model is consistent with the inference that the low amounts of Zn-bearing minerals in natural drainage samples reflect that LDH formation is highly pH- and redox-dependent. Our experiments, coupled with geochemical modelling, indicate the formation of particles similar to a Fe^{2+}–Fe^{3+}–CO_3^{2-}
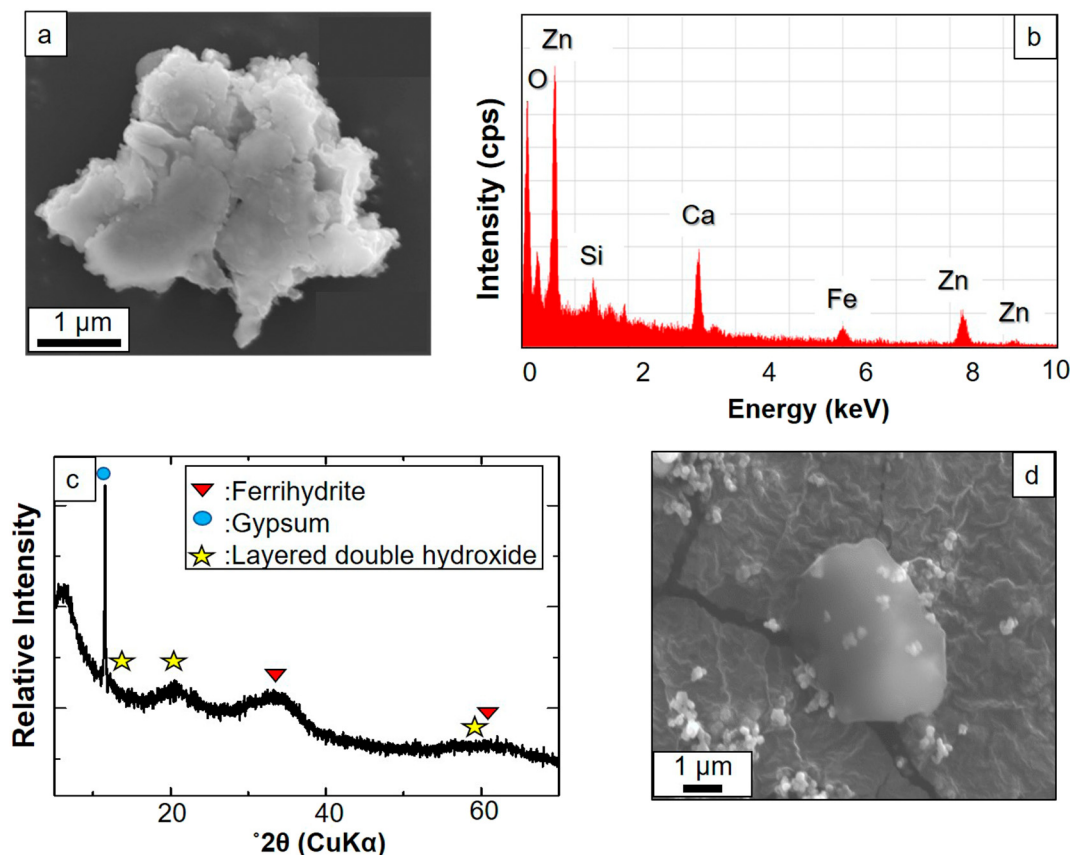
Fig. 7. Field emission SEM images of Zn LDH in (a) aggregates of Fe colloids of a natural sample from S3 suspended solids; and (b) EDS pattern of the Zn-Fe LDH from the natural sample (c) XRD peak of suspended particles collected at S5 and (d) an image of the synthesized Zn-Fe LDH sample.

LDH that incorporate a considerable amount of Fe^{2+} from the source, which later incorporate Zn to form Zn-Fe LDH.

4. Conclusions

This study provides insights into the importance of nanomaterials such as Fe colloids and LDHs for sequestration of toxic elements in

Fig. 8. Stability diagram of Fe species in Ainai mine drainage, based on the chemical composition of the water sample at S2. Lines in the diagrams symbolize the equivalence state between two phases.

circumneutral mine drainage. Our understanding of the formation of these nanomaterials highlights the geochemical properties and processes that play important roles in mine drainage and might be applicable to the treatment of drainage from other mines. A supply of Fe^{2+} from underground wastewater promotes the formation of spherical, homogenous ~100 nm Fe colloids that are micro-aggregates of core–shell ferrihydrite, which co-precipitate with As thereby facilitating the removal of As. Minor Fe concentration variations significantly affect the inverse relationship between Fe and As, especially in terms of colloid size, with a minimal decrease in Fe concentration in October significantly increasing the As concentration. We have established that the mobility of elements depends highly on the size of colloids, which is significantly affected by the aggregation rate. Fe colloids are mobilized for longer in the drainage until aggregating to about 300 μm in size, when they are gravitationally separated. Precipitation and flow rate affect colloid interaction and thereby provide first-order controls on aggregation and deposition, so these parameters should be closely monitored in passive treatment systems.

The application of LDHs as sequestration agents has been explored previously (Wang et al., 2014). Zn is reportedly a challenging element to remediate in natural systems due to its high solubility and poor adsorption onto minerals such as hydroxides and carbonates. Here a novel approach involving isomorphous incorporation of Zn onto an existing Fe^{2+}–Fe^{3+}–CO_3^{2-} LDH to form a Zn-Fe LDH is demonstrated using geochemical modelling, synthetic samples, and observations of natural samples. A combination of high Zn and Fe concentrations and pH > 7.5 is ideal for efficient removal of Zn in passive treatment systems, with Zn-Fe LDH nanoparticles predominating in naturally treated mine drainage.

Critical geochemical factors for heavy-metal removal include wastewater chemistry and composition, pH, flow rate, and aggregation rate.
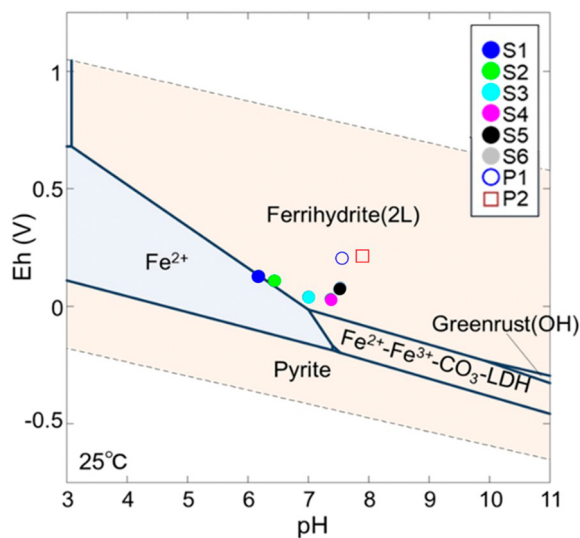
Understanding of these factors enables the role of turbidity and sequestration mechanisms to be clarified. Our findings imply that quantitative prediction of the behavior of nanoparticles such as colloids and LDHs might facilitate optimal design of highly efficient treatment systems, have general applications to mine drainage and other aquatic systems, and improve our understanding of the interaction between toxic elements and colloids that form in these systems.

CRediT authorship contribution statement

Frances Chikanda: Conceptualizations, field and laboratory investigations, formal analyses, writing-original draft. **Tsubasa Otake**: Conceptualizations, investigations, data analyses, validations, review and editing. **Aio Koide**: Conceptualizations, field and laboratory investigations, data analysis and discussions. **Akane Ito**: Conceptualizations, field and laboratory investigations, data analyses and discussions. **Tsutomu Sato**: Conceptualizations, investigations, formal analyses, review and editing, validations.

Declaration of competing interest

The authors declare that they have no known competing or conflict of interest that may have influenced the work reported.

Acknowledgements

Appendix A. Supplementary data

Supplementary data to this article can be found online at https://doi.org/10.1016/j.scitotenv.2021.145183.

References

Akashima, R.N., Araguchi, T.H., Anaka, A.T., 2011. Classification of groundwater according to water quality in Saga Prefecture. Bul. Fac. Agric. Saga. Univ. 97, 27–35.

Allada, R.K., Peltier, E., Navrotsky, A., Casey, W.H., Johnson, C.A., Berbeco, H.L., Sparks, D.L., 2006. Calorimetric determination of the enthalpies of formation of hydrotalcite-like solids and their use in the geochemical modeling of metals in natural waters. Clay Clay Miner. 54, 409–417. https://doi.org/10.1346/CCMN.2006.0540401.

Baalousha, M., 2009. Aggregation and disaggregation of iron oxide nanoparticles: influence of particle concentration, pH and natural organic matter. Sci. Total Environ. 407, 2093–2101. https://doi.org/10.1016/j.scitotenv.2008.11.022.

Bravo-Suárez, J.J., Páez-Mozo, E.A., Oyama, S.T., 2004. Models for the estimation of thermodynamic properties of layered double hydroxides: application to the study of their anion exchange characteristics. Quim Nova 27, 574–581. https://doi.org/10.1590/S0100-40422004000400011.

Buffle, I., Leppard, G.G., 1995. Characterization of aquatic colloids and macromolecules. 1. Structure and behavior of colloidal material. Environ. Sci. Technol. 29, 2169–2175. https://doi.org/10.1021/es00009a004.

Crawford, R.J., Harding, I.H., Mainwaring, D.E., 1993. Adsorption and coprecipitation of multiple heavy metal ions onto the hydrated oxides of Iron and chromium. Langmuir. 9, 3057–3062. https://doi.org/10.1021/la00035a052.

Dold, B., 2014. Evolution of acid mine drainage formation in sulphidic mine tailings. Minerals. 4, 621–641. https://doi.org/10.3390/min4030621.

Dold, B., Fontboté, L., 2002. A mineralogical and geochemical study of element mobility in sulfide mine tailings of Fe oxide Cu-Au deposits from the Punta del Cobre belt, northern Chile. Chem. Geol. 189, 135–163. https://doi.org/10.1016/S0009-2541(02)00044-X.

Fritzsche, A., Rennert, T., Totsche, K.U., 2011. Arsenic strongly associates with ferrihydrite colloids formed in a soil effluent. Environ. Pollut. 159, 1398–1405. https://doi.org/10.1016/j.envpol.2011.01.001.

Fu, F., Wang, Q., 2011. Removal of heavy metal ions from wastewaters: a review. Environ. Manag. 92, 407–418. https://doi.org/10.1016/j.jenvman.2010.11.011.

Gledhiir, M., Buck, K.N., 2012. The organic complexation of iron in the marine environment: a review. Front. Microbiol. 3, 1–17. https://doi.org/10.3389/fmicb.2012.00069.

Hao, L., Liu, M., Wang, N., Li, G., 2018. A critical review on arsenic removal from water using iron-based adsorbents. RSC Adv. 8, 39545–39560. https://doi.org/10.1039/c8ra08512a.

Hase, H., Nishiuchi, T., Sato, Otake, T., Yaita, T., Kobayashi, T., Yoneda, T., 2017. A novel method for remediation of nickel containing wastewater at neutral conditions. J. Hazard. Mater. 329, 49–56. https://doi.org/10.1016/j.jhazmat.2017.01.019.

Hiemenz, P.C., 1972. Proceedings of the California association of chemistry teachers the role of van der Waals forces in surface and colloid chemistry. J. Chem. Educ. 49, 164–170. https://doi.org/10.1021/ed049p164.

Hongo, T., Iemura, T., Yamazaki, A., 2008. Adsorption ability for several harmful anions and thermal behavior of Zn-Fe layered double hydroxide. J. Ceram. 116, 192–197. https://doi.org/10.2109/jcersj2.116.192.

Hunter, R.J., 1963. Van der waals attraction between colloidal particles: the retardation correction for flat plates of arbitrary thickness. Aust. Chem. 16, 774–778. https://doi.org/10.1071/CH9630774.

Ishii, Y., 1964. Geological structures and characteristics of black ore deposits of the ainai mine. J. Mineral. Petro. Econo. Geol. 52, 4.

Japan Meteorological Agency, Japan Meteorological Agency (Eds.), 2018. Climate Change Monitoring Report 2017. Climate in Japan, pp. 16–21 (October).

Jung, H.B., Yun, S., Kwon, J., Zheng, Y., 2012. Role of iron colloids in copper speciation during neutralization in a coastal acid mine drainage, South Korea: insight from voltammetric analyses and surface complexation modeling. J. Geochem. Explor. 112, 244–251. https://doi.org/10.1016/j.gexplo.2011.09.002.

Kellner, R.R., Köhler, W., 2005. Short-time aggregation dynamics of reversible light-induced cluster formation in ferrofluids. J. Appl. Phys. 97. https://doi.org/10.1063/1.1847706.

Khamphila, K., Kodama, R., Sato, T., Otake, T., 2017. Adsorption and post adsorption behavior of schwertmannite with various oxyanions. J. Miner. Mater. Charact. Eng. 05, 90–106. https://doi.org/10.4236/jmmce.2017.52008.

Kirby, C.S., Dennis, A., Kahler, A.K., 2007. Aeration to degas CO₂, increase pH and iron oxidation rates, and decrease treatment pond size in treatment of net alkaline mine drainage. J. ASMR 2, 759–767. https://doi.org/10.21000/jasmr07010373.

Langmuir, D., 1997. Aqueous Environmental Geochemistry. Prentice Hall, New Jersey.

Leupin, O.X., Hug, S.J., 2005. Oxidation and removal of arsenic (III) from aerated groundwater by filtration through sand and zero-valent iron. Water Res. 39, 1729–1740. https://doi.org/10.1016/j.watres.2005.02.012.

Liao, P., Li, W., Wu, J., Jiang, Y., Yuan, S., Fortner, J.D., Glammar, D.E., 2017. Formation, aggregation, and deposition dynamics of nom-iron colloids at anoxic-oxic interfaces. Environ. Sci. Technol. 51, 12235–12245. https://doi.org/10.1021/acs.est.7b02356.

Lu, Q., Bian, Z., Tsuchiya, N., 2019. Hydrotransport-oriented Zn, Cu, and Pb behavior assessment and source identification in the river network of a historically mined area in the Hokuroku basin, Northeast Japan. Int. J Environ. 16, 20. https://doi.org/10.3390/ijerph16203907.

Michel, M.F., 2007. The structure of ferrihydrite, a nanocrystalline material. Science 316, 1726–1729.

Moaty, S.A.A., Farghali, A.A., Khaled, R., 2016. Preparation, characterization and antimicrobial applications of Zn-Fe LDH against MRSA. Mater. Sci. Eng. C 68, 184–193. https://doi.org/10.1016/j.msec.2016.05.110.

Mokhter, M., Magnenet, C., Lakard, S., Euvrard, M., Aden, M., Clement, S., Lakard, B., 2018. Use of modified colloids and membranes to remove metal ions from contaminated solutions. Colloids Interfaces 2, 19. https://doi.org/10.3390/colloids2020019.

Morimoto, K., Tamura, K., Anraku, S., Sato, T., Suzuki, M., Yamada, H., 2015. Synthesis of Zn-Fe layered double hydroxides via an oxidation process and structural analysis of products. J. Solid State Chem. 228, 221–225. https://doi.org/10.1016/j.jssc.2015.04.045.

Nairn, R.W., O'Sullivan, A.D., Coffey, J., 2002. Iron oxidation in net alkaline CO₂-rich mine waters. JASMR 2002, 1133–1137. https://doi.org/10.21000/jasmr02011133.

Nguyen, K.M., Nguyen, B., Hai, N.T., Nguyen, T.H.H., 2019. Adsorption of arsenic and heavy metals from solutions by unmodified iron-ore sludge. Appl. Sci. 9 (4). https://doi.org/10.3390/app9040619.

Nordstrom, D.K., 2011. Mine waters: acidic to Circumneutral. Geol. 393–398. https://doi.org/10.2113/gselements.7.6.393.

Okamoto, H., Morimoto, K., Anraku, S., Sato, T., Yoneda, T., 2010. A novel remediation method learnt from natural attenuation process for Cu- and Zn-bearing wastewater. Clay Sci. 14, 203–210. https://doi.org/10.11362/jcssjclayscience.14.5_203.

Parida, K.M., Mohapatra, L., 2012. Carbonate intercalated Zn/Fe layered double hydroxide: a novel photocatalyst for the enhanced photo degradation of azo dyes. Chem. Eng. J. 179, 131–139. https://doi.org/10.1016/j.cej.2011.10.070.

Petosa, A.R., Jaisi, D.P., Quevedo, I.R., Elimelech, M., Tufenkji, N., 2010. Aggregation and deposition of engineered nanomaterials in aquatic environments: role of physicochemical interactions. Environ. Sci. Technol. 44, 6532–6549. https://doi.org/10.1021/es100598h.

Plumlee, G.S., Logsdon, M.J., Filipek, L.F., 1997. Metal sorption on mineral surfaces. Econ. Geol. 6, 161–182. https://doi.org/10.5382/rev.06.07.

Pokrovsky, O.S., Schott, J., 2002. Iron colloids/organic matter associated transport of major and trace elements in small boreal rivers and their estuaries (NW Russia). Chem. Geol. 190, 141–179. https://doi.org/10.1016/S0009-2541(02)00115-8.

Rezaei, M., Poureshgh, Y., Fatehizadeh, A., Shahriary, A., Toolabi, A., Rezaei, M., 2013. Annual and seasonal variation of turbidity, total dissolved solids, nitrate and nitrite in the Parsabad water treatment plant, Iran. Int. J. Environ. Health Eng. 2, 37. https://doi.org/10.4103/2277-9183.122421.

Roberts, D.R., Scheinost, A.C., Sparks, D.L., 2002. Zinc speciation in a smelter-contaminated soil profile using bulk and microspectroscopic techniques. Environ. Sci. Technol. 36, 1742–1750. https://doi.org/10.1021/es015516c.

Rounds, S.A., Wilde, F.D., 2006. Alkalinity and Acid Neutralizing Capacity. 3. US Geological Survey, pp. 1–53. https://doi.org/10.3133/twri09A6.6.

Schemel, L.E., Kimball, B.A., Bencala, K.E., 2000. Colloid formation and metal transport through two mixing zones affected by acid mine drainage near Silverton, Colorado. Appl. Geochem. 15, 1003–1018. https://doi.org/10.1016/S0883-2927(99)00104-3.

Sharma, P., Ofner, J., Kappler, A., 2010. Formation of binary and ternary colloids and dissolved complexes of organic matter, Fe and As. Environ. Sci. Technol. 44, 4479–4485. https://doi.org/10.1021/es100066s.

Stumm, W., Morgan, J.J., 2006. Aquatic Chemistry. third edition. John Wiley and Sons.

Tikhonova, T.N., 2016. The role of colloid particles in the albumin-lanthanides interaction: the study of aggregation mechanisms. Colloids Surf B. 146, 507–513. https://doi.org/10.1016/j.colsurfb.2016.06.049.

Vempati, R.K., Loeppert, R.H., Cocke, D.L., 1990. Mineralogy and reactivity of amorphous Si-ferrihydrites. Solid State Ionics 38, 53–61. https://doi.org/10.1016/0167-2738(90)90443-U.

Wang, Q., Cheng, T., Wu, Y., 2014. Influence of mineral colloids and humic substances on uranium(VI) transport in water-saturated geologic porous media. J. Contam. Hydrol. 170, 76–85. https://doi.org/10.1016/j.jconhyd.2014.10.007.

Weatherill, J.S., 2016. Ferrihydrite formation: the role of Fe13 Keggin clusters. Environ. Sci. Technol. 50, 9333–9342. https://doi.org/10.1021/acs.est.6b02481.

Whitney King, D., 1998. Role of carbonate speciation on the oxidation rate of Fe(II) in aquatic systems. Environ. Sci. Technol. 32, 2997–3003. https://doi.org/10.1021/es980206o.

Xu, Y., 2013. Sorption of metal cations on layered double hydroxides. Colloids Surf. 433, 122–131. https://doi.org/10.1016/j.colsurfa.2013.05.006.

Yamada, R., Yoshida, T., 2011. Relationships between Kuroko volcanogenic massive sulfide (VMS) deposits, felsic volcanism, and island arc development in the Northeast Honshu arc, Japan. Mineral. Deposita 46, 431–448. https://doi.org/10.1007/s00126-011-0362-7.

Yao, M., Nan, J., Chen, T., 2014. Effect of particle size distribution on turbidity under various water quality levels during flocculation processes. Desalin. 354, 116–124. https://doi.org/10.1016/j.desal.2014.09.029.

Yokoyama, T., Makishima, A., Nakamura, E., 1999. Evaluation of the coprecipitation of incompatible trace elements with fluoride during silicate rock dissolution by acid digestion. Chem. Geol. 157, 175–187. https://doi.org/10.1016/S0009-2541(98)00206-X.

Zaher, A., 2020. Zn/Fe LDH as a clay-like adsorbent for the removal of oxytetracycline from water: combining experimental results and molecular simulations to understand the removal mechanism. Environ. Sci. Pol. 27, 12256–12269. https://doi.org/10.1007/s11356-020-07750-3.

Zay Ya, K., Otake, T., Koide, A., Sanematsu, K., Sato, T., 2020. Geochemical characteristics of ores and surface waters for environmental risk assessment in the Pinpet iron deposit, southern Shan State, Myanmar. Resour. Geol. 70, 1–13. https://doi.org/10.1111/rge.12231.

Zeng, L., 2003. A method for preparing silica-containing iron(III) oxide adsorbents for arsenic removal. Water Res. 37, 4351–4358. https://doi.org/10.1016/S0043-1354(03)00402-0.

Zhao, Z., Jia, Y., Xu, L., Zhao, S., 2011. Adsorption and heterogeneous oxidation of As(III) on ferrihydrite. Water Res. 45, 6496–6504. https://doi.org/10.1016/j.watres.2011.09.051.

Zipper, C., Skousen, J., 2014. Passive treatment of acid mine drainage. In: Jacobs, J.A., Lehr, J.H., Testa, S.M. (Eds.), Acid Mine Drainage, Rock Drainage, and Acid Sulfate Soils: Causes, Assessment, Prediction, Prevention, and Remediation. 9780470487, pp. 339–353. https://doi.org/10.1002/9781118749197.ch30.